Functional Redundancy and Divergence within the Arabidopsis RETICULATA-RELATED Gene Family[1][W][OA]

José Manuel Pérez-Pérez, David Esteve-Bruna[2], Rebeca González-Bayón[2,3], Saijaliisa Kangasjärvi, Camila Caldana[4], Matthew A. Hannah[5], Lothar Willmitzer, María Rosa Ponce, and José Luis Micol*

Instituto de Bioingeniería, Universidad Miguel Hernández, Campus de Elche, 03202 Elche, Alicante, Spain (J.M.P.-P., D.E.-B., R.G.-B., M.R.P., J.L.M.); Department of Biochemistry and Food Chemistry, University of Turku, FI–20014 Turku, Finland (S.K.); and Max-Planck-Institute of Molecular Plant Physiology, 14476 Potsdam-Golm, Germany (C.C., M.A.H., L.W.)

A number of Arabidopsis (*Arabidopsis thaliana*) mutants exhibit leaf reticulation, having green veins that stand out against paler interveinal tissues, fewer cells in the interveinal mesophyll, and normal perivascular bundle sheath cells. Here, to examine the basis of leaf reticulation, we analyzed the Arabidopsis RETICULATA-RELATED (RER) gene family, several members of which cause leaf reticulation when mutated. Although transcripts of *RE*, *RER1*, and *RER3* were mainly detected in the bundle sheath cells of expanded leaves, functional RER3:GREEN FLUORESCENT PROTEIN was visualized in the chloroplast membranes of all photosynthetic cells. Leaf reticulation in the *re* and *rer3* loss-of-function mutants occurred, along with accumulation of reactive oxygen species, in a photoperiod-dependent manner. A comparison of *re* and *rer3* leaf messenger RNA expression profiles showed more than 200 genes were similarly misexpressed in both mutants. In addition, metabolic profiles of mature leaves revealed that several biosynthetic pathways downstream of pyruvate are altered in *re* and *rer3*. Double mutant analysis showed that only *re rer1* and *rer5 rer6* exhibited synergistic phenotypes, indicating functional redundancy. The redundancy between *RE* and its closest paralog, *RER1*, was confirmed by overexpressing *RER1* in *re* mutants, which partially suppressed leaf reticulation. Our results show that RER family members can be divided into four functional modules with divergent functions. Moreover, these results provide insights into the origin of the reticulated phenotype, suggesting that the RER proteins functionally interconnect photoperiodic growth, amino acid homeostasis, and reactive oxygen species metabolism during Arabidopsis leaf growth.

Leaf development requires the complex coordination of morphogenetic and metabolic factors for the specification and differentiation of tissue types with distinct functions. This process can be probed by detailed examination of informative mutant phenotypes; for example, a number of reticulate mutants with leaves exhibiting a green vascular pattern on a paler lamina have been described (Li et al., 1995; Kinsman and Pyke, 1998; González-Bayón et al., 2006; Mollá-Morales et al., 2011). The interveinal regions of their reticulate leaves always contain fewer and smaller mesophyll cells than those of the wild type; in many cases, this phenotype also includes altered plastid number, size, and/or differentiation status. These observations suggest that a number of reticulate mutants are impaired in retrograde signaling, the signals that an organelle emits to regulate the expression of nuclear genes (Fernández and Strand, 2008), from the chloroplasts to the cell nucleus, which in turn affects mesophyll growth and development (Yu et al., 2007). Alternatively and because the differentiation of bundle sheath cells precedes mesophyll differentiation (Kinsman and Pyke, 1998), a limited supply of essential metabolites in early stages of leaf development might cause the aberrant mesophyll structure of some reticulate mutants due to developmental constraints (Rosar et al., 2012).

Examination of these reticulated mutants has shed light on the contribution of metabolic factors to leaf morphology. For example, amino acid metabolism is altered in the *chlorophyll a/b binding protein underexpressed* (*cue1*), *reticulata* (*re*), *venosa3* (*ven3*), and *ven6* reticulate Arabidopsis (*Arabidopsis thaliana*) mutants. *CUE1*

[1] This work was supported by the Ministerio de Economía y Competitividad of Spain (grant nos. BFU2011–22825 and CSD2007–00057 to J.L.M.; TRANSPLANTA), the Generalitat Valenciana (grant no. PROMETEO/2009/112 to J.L.M. and fellowship no. BFPI/2009/015 to D.E.-B.), the European Commission (grant no. LSHG–CT–2006–037704 to L.W. and J.L.M.; AGRON-OMICS), and the Academy of Finland (decision nos. 218157 and 130595 to S.K.).

[2] These authors contributed equally to the article.

[3] Present address: Plant Industry, Commonwealth Scientific and Industrial Research Organization, Canberra, ACT 2600, Australia.

[4] Present address: Brazilian Bioethanol Science and Technology Laboratory (Centro Nacional de Pesquisa em Energia e Materiais/Associação Brasileira de Tecnologia de Luz Síncrotron), Rua Giuseppe Máximo Scolfano 10000, 13083–970, Campinas, Brazil.

[5] Present address: Bayer CropScience N.V., Technologiepark 38, 9052 Ghent, Belgium.

* Corresponding author; e-mail jlmicol@umh.es.

The author responsible for distribution of materials integral to the findings presented in this article in accordance with the policy described in the Instructions for Authors (www.plantphysiol.org) is: José Luis Micol (jlmicol@umh.es).

[W] The online version of this article contains Web-only data.

[OA] Open Access articles can be viewed online without a subscription.

www.plantphysiol.org/cgi/doi/10.1104/pp.113.217323

encodes a phospho*enol*pyruvate (PEP)/phosphate antiporter located on the chloroplast inner membrane (Fischer et al., 1997). PEP is synthesized in the cytosol and is used in the chloroplasts for the biosynthesis of aromatic amino acids and other derived compounds through the shikimate pathway (Knappe et al., 2003). Arabidopsis *VEN3* and *VEN6* encode the two subunits of carbamoyl phosphate synthetase (CPS), which is required in the chloroplasts for Arg biosynthesis (Mollá-Morales et al., 2011).

Intriguingly, in reticulate leaves, the interveinal regions show smaller and fewer cells, but the bundle sheath cells do not appear to be affected. In C_4 plants, bundle sheath cells have a characteristic morphology, spatial localization, and photosynthetic function. When compared with the system that operates in C_4 plants, the photosynthetic cells that surround the vascular bundle in C_3 plants show striking parallelisms (Hibberd and Quick, 2002). Arabidopsis is a typical C_3 plant, but it also has bundle sheath cells (Kinsman and Pyke, 1998; Leegood, 2008). On the one hand, similar to VEN3 in Arabidopsis (Potel et al., 2009), CPS in maize (*Zea mays*) leaves is found at higher levels in the bundle sheath cells than in the interveinal palisade mesophyll cells (Friso et al., 2010), suggesting that the pool of CPS, and thus that of Arg, may be higher in bundle sheath cells than in the interveinal mesophyll in both species. On the other hand, reducing chlorophyll biosynthesis specifically in the bundle sheath cells of Arabidopsis leaves (Janacek et al., 2009) causes both a reduction of soluble sugars and of carbon skeletons that fuel the shikimate pathway in these cells, which also confirms the existence of specific biochemical pathways in bundle sheath cells and palisade mesophyll cells in C_3 plants, as previously proposed (Hibberd and Quick, 2002).

Here, we analyze loss-of-function mutants of five members of the RETICULATA-RELATED (RER) gene family, named for its founding member, *RETICULATA* (Barth and Conklin, 2003; González-Bayón et al., 2006). The synergistic or additive phenotypes of different double mutant combinations suggest both functional redundancy and specialization of RER functions during leaf growth. The metabolic profiles of *re* and *rer3* mutants revealed alterations in several biosynthetic pathways downstream of pyruvate, which is in agreement with the hypothesis that a limited supply of essential metabolites in the mesophyll during early leaf development is the cause for their reticulate phenotypes. This comprehensive examination of the RER gene family therefore reveals redundancy and specialization in RER function and sheds light on the complex connection between leaf development and metabolism in the development of the reticulated phenotype.

RESULTS

Genes of the RER Family Encode Chloroplast-Targeted Proteins

Work on single reticulate mutants has provided some insights into the nature of the reticulate phenotype; to extend these results, we examined a related gene family. The first mutant with reticulate leaves isolated in Arabidopsis was *re* (Rédei and Hirono, 1964). Loss-of-function mutations of *RE*, which encodes a protein of unknown function, cause increased sensitivity to ozone (Barth and Conklin, 2003) and specifically reduce mesophyll cell numbers in the early stages of leaf organogenesis (González-Bayón et al., 2006). We identified six Arabidopsis genes encoding proteins with high sequence similarity to RE (Fig. 1A; Supplemental Fig. S1) and named these genes *RER1* to *RER6* (Table I). The RER family is plant specific, and its members are present in all plant genomes sequenced so far. Based on gene structure and amino acid sequence similarity, RER proteins (Fig. 1B) can be grouped into three pairs, RE-RER1, RER2-RER3, and RER5-RER6, and one single protein, RER4. The predicted RER2 and RER3 proteins show 84% amino acid sequence identity, and *RER2* (At3g08630) and *RER3* lack introns and are arranged in tandem, suggesting that they arose from a recent duplication event. Several studies have identified most RER family proteins as integral components of the chloroplast envelope (Ferro et al., 2003, 2010; Froehlich et al., 2003; Kleffmann et al., 2004; Dunkley et al., 2006; Zybailov et al., 2008). All proteins of the RER family contain a plant-specific, conserved amino acid domain of unknown function, DUF3411 (Supplemental Fig. S1). In silico prediction of transmembrane (TM) domains revealed two conserved TM α-helixes, TM1 and TM2, within the DUF3411 motif and another one, TM3, in the C-terminal region of RER2, RER3, and RER4 (Supplemental Fig. S1), which is consistent with their localization in the membrane. By contrast, RER5 and RER6 were the most divergent members of the family, because they also contained a DUF399 domain (Supplemental Fig. S1) and have been identified in the thylakoid lumen proteome (Peltier et al., 2002; Schubert et al., 2002).

Loss-of-Function Alleles of *RE*, *RER3*, and *RER4*, But Not *RER1*, *RER5*, and *RER6*, Cause Leaf Reticulation

To examine the functions of these genes, we next identified and characterized loss-of-function mutant alleles. From available collections of gene-indexed insertion lines (Sessions et al., 2002; Alonso et al., 2003; Li et al., 2007), we identified homozygous lines containing a transfer DNA (T-DNA) insertion in each of the *RER* genes, except *RER2* and *RER3* (Table I; Fig. 1A). *RER1* transcript levels, as measured by quantitative reverse transcription (RT)-PCR, were severely reduced in the *rer1-1* mutant (Supplemental Fig. S2). However, the rosette and leaf phenotypes of three *rer1* homozygous mutants were indistinguishable from those of wild-type plants of their Columbia (Col-0) genetic background (Fig. 1, C and F; data not shown). Adaxial epidermis and palisade mesophyll histology, as well as vein patterning, seemed unaffected by the *rer1* mutations (Fig. 2, A–C). We did not observe any differences from the wild type in *rer1* homozygous roots, inflorescences, flowers, or siliques (data not shown).

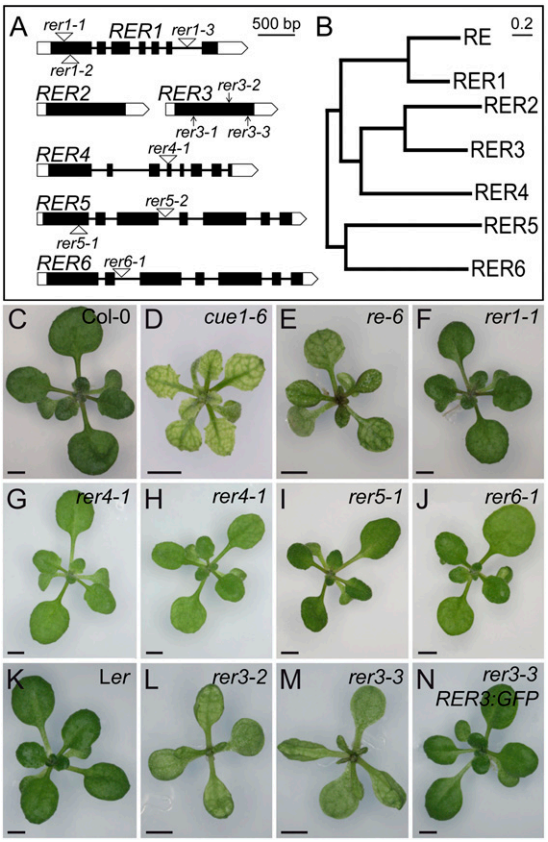

Figure 1. The RER gene family. A and B, Structure and phylogenetic tree of the genes of the RER family. A, Exons are indicated by boxes and introns by lines between boxes. Coding and untranslated regions are shown as black and white boxes, respectively. T-DNA insertions are indicated as white triangles, and point mutations are indicated as arrows. B, Neighbor-joining tree of RER protein sequences constructed with MEGA5.1. Bar = 20% amino acid sequence changes. C to N, Rosette phenotypes of the *re* and *rer* mutants. The Col-0 (C) and L*er* (K) wild types and the *cue1-6* reticulate mutant (D) are included for comparison. The T-DNA insertional lines shown are *re-6* (E), *rer1-1* (F), *rer4-1* grown under standard light conditions (80 μmol m^{-2} s^{-1}; G) or low light fluence rate conditions (54 μmol m^{-2} s^{-1}; H), *rer5-1* (I), and *rer6-1* (J). The reticulate phenotype of *rer3-2* (L) and *rer3-3* (M), whose genetic background is L*er*, is rescued by the *RER3*$_{pro}$*:RER3:GFP* transgene (N). Pictures were taken 14 das. Bars = 2 mm (C–N).

A T-DNA insertion allele of *RER4*, *rer4-1* (Table I), reduced the *RER4* mRNA levels significantly (Supplemental Fig. S2) and caused subtle leaf lamina reticulation and reduced leaf growth, phenotypes that were only obvious under low light fluency (Fig. 1, G and H). We identified two T-DNA insertion alleles of *RER5* and one of *RER6* (Table I), which also showed significantly reduced mRNA levels (Supplemental Fig. S2). As seen in the *rer1* mutants, leaves and rosettes of *rer5-1*, *rer5-2*, and *rer6-1* were phenotypically wild type in all conditions tested (Fig. 1, I and J; data not shown).

The three *ven5* mutants isolated previously (Berná et al., 1999) also display reticulate leaves (Fig. 1, L and M). A total of 170 phenotypically recessive F2 plants derived from a *ven5-3* × Col-0 cross were used as a mapping population for linkage analysis, which allowed us to delimit a 400-kb region near the upper telomere of chromosome 3; this region includes both *RER2* and *RER3*. We sequenced both genes in the *ven5* mutants and in their wild-type Landsberg *erecta* (L*er*) ecotype and found G→A transitions in the *RER3* coding region in all *ven5* mutants. *ven5-1* changes Gly-129 to Glu, *ven5-3* changes Gly-228 to Ser, and *ven5-2* carries a nonsense mutation that changes Trp-262 to a premature stop codon, which would produce a truncated protein lacking 76 residues of its C terminus. All these mutations affect conserved residues in the DUF3411 protein domain (Supplemental Fig. S1). Because *ven5-1*, *ven5-3*, *and ven5-2* were found to be alleles of *RER3*, we renamed them as *rer3-1*, *rer3-2*, and *rer3-3*, respectively (Table I).

Similar to other reticulate mutants (Fig. 1, D and E; González-Bayón et al., 2006; Horiguchi et al., 2011; Mollá-Morales et al., 2011), *rer3-1*, *rer3-2*, and *rer3-3* homozygotes characteristically displayed green tissues surrounding the veins and a paler leaf lamina (Fig. 1, L and M). The *rer3* mutations also caused mild leaf hyponasty and deep indentations on the leaf margin, both traits being obvious at all stages of leaf expansion (data not shown). Paradermal differential interference contrast (DIC) micrographs showed a disorganized mesophyll with increased air spaces in *rer3* cotyledons and leaves (Fig. 2, G and H). All *rer3* mutants showed a strong reduction in cell area and in the lobe sizes of their adaxial epidermal pavement cells (Fig. 2, G and H). These results indicate that in *rer3* mutant leaves, cell number is reduced in the mesophyll and cell expansion is reduced in the epidermis. Consistent with reduced cell expansion, the 8C and 16C nuclei populations of the first leaf pair at 14 and 21 d after stratification (das) were lower in *rer3* than in L*er*, similar to that found for the strong reticulate mutant *cue1-6* (Supplemental Table S1). Transgenic *rer3-3* homozygous plants expressing the *RER3*$_{pro}$*:RER3:GFP* construct (Fig. 1N) had leaves indistinguishable from those of L*er* (Fig. 1K), thus confirming that all the phenotypes displayed by the *rer3* mutants are caused by loss of function of the *RER3* gene.

RER3 Is Specifically Required for Embryogenesis

In addition to identifying redundant functions in the RER family, we also looked for specific or divergent functions. We found that in addition to the reticulated phenotype of their leaves (Fig. 1, L and M), the *rer3* alleles described in this work caused additional defects in seedling germination and early growth. To look for embryonic patterning defects, we dissected siliques of the *rer3* mutants and found a high proportion (48%) of aberrant embryos. In some cases, globular embryos contained two cell rows in the suspensor (Fig. 3A), as opposed to the single row of cells found in the wild type (Fig. 3C). In many cases, the heart embryo stage

Table I. *Mutant alleles of RER family genes studied in this work*
EMS, Ethyl methanesulfonate; ∇, T-DNA insertion.

Gene	Arabidopsis Genome Initiative Code	Allele	Alternative Allele Name/Line	Genetic Background	Mutagen	Mutation and Effects[a]	Origin[b]
RE	AT2G37860	*re-3*	*ven2-1*	L*er*	EMS	G1658→A (Gly-328→Arg)	1, 2
		re-4	*ven2-2*	L*er*	EMS	C1378→T (Pro-295→Leu)	1, 2
		re-6	Salk_084529	Col-0	T-DNA	∇113 (second exon)	2
		re-8	*rcd2*	Col-0	EMS	G→A (5th intron splice acceptor site, truncated protein)	3
RER1	AT5G22790	*rer1-1*	Salk_126363	Col-0	T-DNA	∇239 (first exon)	4
		rer1-2	Salk_073984	Col-0	T-DNA	∇339 (first exon)	4
		rer1-3	Salk_093173	Col-0	T-DNA	∇1704 (sixth intron)	4
RER3	AT3G08640	*rer3-1*	*ven5-1*	L*er*	EMS	G386→A (Gly-129→Glu)	1, 4
		rer3-2	*ven5-3*	L*er*	EMS	G682→A (Gly-228→Ser)	1, 4
		rer3-3	*ven5-2*	L*er*	EMS	G785→A (Trp-262→STOP)	1, 4
RER4	AT5G12470	*rer4-1*	Sail_1235_D10	Col-0	T-DNA	∇1512 (fourth exon)	4
RER5	AT2G40400	*rer5-1*	Salk_116717	Col-0	T-DNA	∇482 (first exon)	4
		rer5-2	Salk_082660	Col-0	T-DNA	∇1607 (third intron)	4
RER6	AT3G56140	*rer6-1*	Salk_111366	Col-0	T-DNA	∇926 second intron)	4

[a]Numbers refer to nucleotides in genomic DNA, starting from position +1 of the transcription unit, and amino acids in the predicted protein. [b]1, Berná et al., 1999; 2, González-Bayón et al., 2006; 3, Overmyer et al., 2008; 4, This study.

of the *rer3* mutants showed clear asymmetries in their apical domains (Fig. 3B). For the seeds that germinated, 18% of *rer3* homozygotes showed an abortive seedling phenotype, characterized by dark-green small rosettes that do not develop roots (Fig. 3, E and F). Moreover, 12% to 25% of the *rer3* rosettes with reticulate leaves contained only one cotyledon, with the first-node leaf arising opposite to it (Fig. 3G). In 5% to 10% of these plants, the first two leaves were fused (Fig. 3H). However, for seedlings that developed roots, we found no significant differences in the length of the primary root of either *rer3* or *re-3* mutants compared with L*er*. Also, the morphology of their distal root meristem did not differ between the *re* or *rer3* mutants and their wild-type L*er* (data not shown).

As the *rer3* embryogenesis defect is similar to mutants affected in auxin signaling, we visualized the expression of the *DR5rev*:*GFP* auxin reporter (Benková et al., 2003) during embryogenesis. In embryos at the torpedo stage, we found only a peak of *DR5rev*:*GFP* expression in the most distal cells of the embryo, both in the wild type (96.9%, $n = 32$; Supplemental Fig. S3A) and *re-3* (92.3%, $n = 26$; Supplemental Fig. S3B), as well as in *rer3-3* embryos displaying a wild-type phenotype (92.9%, $n = 28$; Supplemental Fig. S3C). However, most of the aberrant *rer3-3* embryos analyzed (78.3%, $n = 23$) expressed the reporter gene also in the apical cells of the embryo proper (Supplemental Fig. S3, D and E). Postembryonically, *DR5rev*:*GFP* expression was found increased in leaf primordia and in root tips of *rer3-3* (Supplemental Fig. S3, H and K), above that found in their wild-type L*er* (Supplemental Fig. S3, F and I) and *re-3* mutants (Supplemental Fig. S3, G and J). Taken together, our results suggest that *RER3* is specifically required for embryogenesis in concert with auxin.

The Expression Patterns of RER Family Genes Partially Overlap

To further characterize the functions of RER family members, we examined the expression patterns of each gene, gathering information on the temporal and spatial expression of RER family members from publicly available microarray data (Schmid et al., 2005; Supplemental Fig. S4). The expression levels of *RE* and *RER1* in different organs and developmental stages were comparable in the studied data set. Expression of *RER3* mostly mirrored that of *RER2*, although *RER3* was highly expressed in seeds and specifically in the late stages of embryo development. *RER5* and *RER6* were similarly expressed, except in mature pollen and young leaves, where *RER5* expression was higher than that of *RER6*. For each gene of the RER family, we retrieved the most significantly coexpressed genes from the ATTED-II database; several genes encoding enzymes involved in amino acid biosynthesis were coexpressed only with *RER3* (Supplemental Fig. S5).

We then examined the spatial expression pattern of *RE*, *RER1*, and *RER3* using transcriptional fusions of their upstream regulatory sequences to the *β-glucuronidase* (*GUS*) gene. *RE* was predominantly expressed in the proximal region of young leaf primordia (Fig. 4A). By contrast, *RER1* was expressed in the distal region of young leaf primordia (Fig. 4F). Expression of *RE* and *RER1* partially overlapped in developing leaves (Fig. 4, B and G), whereas in mature leaves their expression was indistinguishable (Fig. 4, C and H) and restricted to some cells associated with the vasculature (i.e. bundle sheath cells; Fig. 4, D and I) and the hydathodes (Fig. 4, E and J). Similar to *RER1*, the highest *RER3* expression was observed in the distal region of young leaf primordia (Fig. 4K). In developing and fully expanded leaves, *RER3* expression was higher in

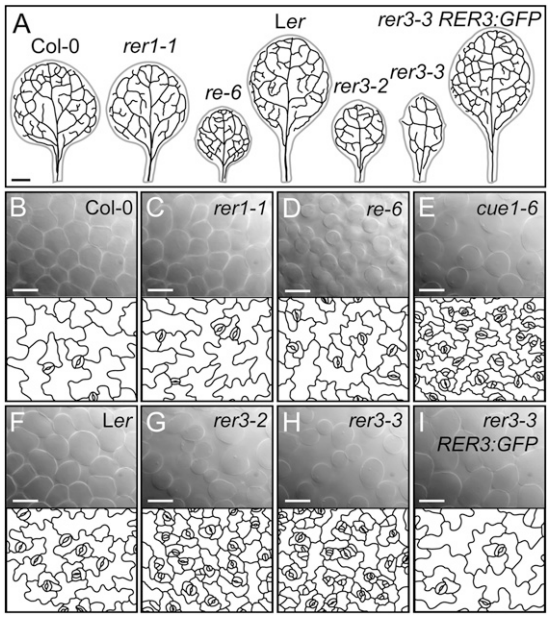

Figure 2. Leaf histology of the *re* and *rer* mutants. A, Venation patterns of the first pair of leaves of Col-0, *rer1-1*, *re-6*, L*er*, *rer3-2*, *rer3-3*, and a transgenic line expressing the *RER3*$_{pro}$:*RER3*:*GFP* in a *rer3-3* background. B to I, Palisade mesophyll DIC micrographs (top) and representative diagrams from the leaf adaxial epidermis of *rer* mutants (bottom, window size: 210 × 165 μm), which were drawn from DIC micrographs of first- or second-node cleared leaves harvested 14 das from Col-0 (B), *rer1-1* (C), *re-6* (D), *cue1-6* (E), L*er* (F), *rer3-2* (G), *rer3-3* (H), and *rer3-3* expressing the *RER3*$_{pro}$:*RER3*:*GFP* transgene (I). Bars = 1 mm (A) and 40 μm (B–I).

the bundle sheath cells and the hydathodes than in other tissues (Fig. 4, L–O). Paradermic sections of mature leaves excised from *RE*$_{pro}$:*GUS* and *RER3*$_{pro}$:*GUS* transgenic lines confirmed the higher expression of these genes in the bundle sheath cells (Fig. 4D). In the root meristem, *RE* expression was high in tier 1 of the columella in the stem cell niche (Supplemental Fig. S6A), where *RER1* expression was undetectable (Supplemental Fig. S6B). Interestingly, *RER3* expression was detected in the mitotic pool of the root meristem (Supplemental Fig. S6C). In the differentiation zone of roots, however, the expression of *RE*, *RER1*, and *RER3* fully overlapped and was restricted to the cells surrounding the vasculature (Supplemental Fig. S6, D–F). Our GUS expression analysis showed that *RE*, *RER1*, and *RER3* were also similarly expressed in pollen (Supplemental Fig. S6G; data not shown), a result that we independently confirmed by in situ hybridization (Supplemental Materials and Methods S1) with a *RE* antisense probe (Supplemental Fig. S6H). During embryogenesis, faint GUS staining was observed from torpedo stage onwards in embryos expressing the *RE*$_{pro}$:*GUS* construct (Supplemental Fig. S6J), whereas no staining was found in *RER1*$_{pro}$:*GUS* embryos (Supplemental Fig. S6K). By contrast, *RER3* expression was higher during embryogenesis, from the heart stage onwards, and was restricted to the adaxial side of the cotyledons (Supplemental Fig. S6L).

To determine the localization of the RER3 protein, we used the *RER3*$_{pro}$:*RER3*:*GFP* construct. In mature leaves, the RER3:GFP fusion protein colocalizes with the chlorophyll autofluorescence from the palisade mesophyll and spongy mesophyll chloroplasts, as well as with the chloroplasts of guard cells and of the hypocotyl (Fig. 4, P–R). RER3:GFP was also detected in the nonphotosynthetic root leucoplasts (Fig. 4S). After chlorophyll bleaching (see "Materials and Methods"), RER3:GFP expression remained confined to the periphery of mature chloroplasts in leaf tissues (Fig. 4, T and U). The GFP signal of the RER3:GFP fusion protein was higher in small, immature plastids (Fig. 4, Q, S, and U, arrows). These results, which were obtained using a functional RER3:GFP protein, demonstrate that RER3 localizes to the chloroplast membranes of all plastid-containing cells.

Several Pairs of Genes of the RER Family Are Functionally Redundant

Based on their protein sequence similarity and expression patterns (see above), we suspected that the *RE* and *RER1* paralog pair might have a redundant role during leaf development. To test this hypothesis, we crossed reticulated *re-3*, *re-4*, and *re-6* mutants to nonreticulated *rer1-1*, *rer1-2*, and *rer1-3* mutants. Among the F2 populations studied, we obtained approximately 10% of mutants displaying the characteristic phenotype described previously for *re* mutants (González-Bayón et al., 2006; Fig. 1E), as well as an additional 2% of seedlings exhibiting stunted rosette growth with small and reticulated leaves (Fig. 5A; Supplemental Table S2). In the absence of genetic

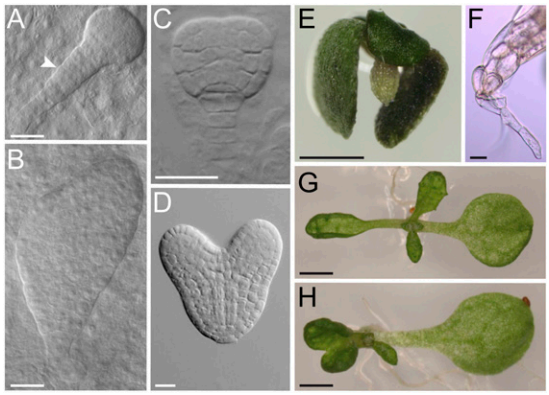

Figure 3. Embryonic and early seedling phenotypes of the *rer3-3* mutant. Aberrant *rer3-3* (A and B) and wild-type embryos (C and D) at the late globular (A and C) and heart (B and D) stages. A white arrowhead in A points to an abnormal suspensor. A *rer3-3* seedling lacking basal structures (E) and details of its hypocotyl showing a single root hair at the tip (F). Some *rer3-3* seedlings display a single cotyledon, either with a single first-node leaf (G) or with fused first-node pair leaves (H). Pictures were taken 45 (A–D) and 7 (E–H) das. Bars = 20 μm (A–D and F) and 1 mm (E, G, and H).

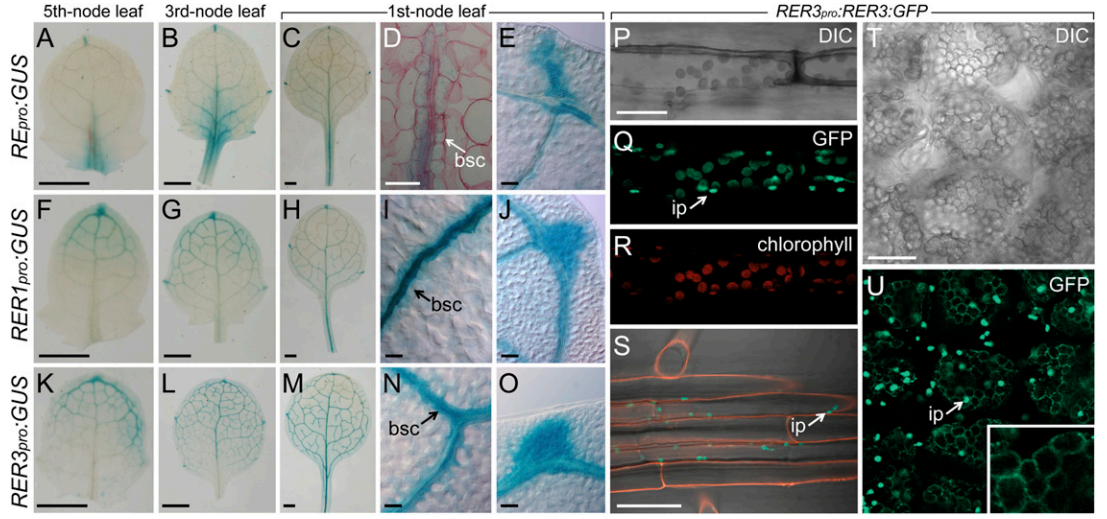

Figure 4. RER gene expression and RER3 protein localization. A to O, Expression of *RE*, *RER1*, and *RER3* in leaves. GUS activity of RE_{pro}:*GUS* (A–E), $RER1_{pro}$:*GUS* (F–J), and $RER3_{pro}$:*GUS* (K–O) transgenic plants in the Col-0 background. Magnifications are shown for the spongy mesophyll (D, I, and N) and lateral hydathodes (E, J, and O). bsc, Bundle sheath cells. P to U, Expression of the RER3:GFP fusion protein. Detail of an epidermal cell from the hypocotyl (P–R), the root epidermis at the differentiation region (S), and cleared palisade mesophyll cells (T and U). Red channel: chlorophyll autofluorescence (R) or propidium iodide staining (S) of cell walls. ip, Immature plastids. Pictures were taken on samples harvested 11 das. Bars = 0.5 mm (A–C, F–H, and K–M), 40 μm (D, E, I, J, N, and O), and 20 μm (P–U).

interaction between *re* and *rer1* mutations, which are unlinked, one would expect about 25% reticulated seedlings in the F2 generation. One hundred and eighty F2 reticulate plants were genotyped and unambiguously found to be *re/re;RER1/RER1*. All the 23 seedlings exhibiting a severe phenotype were *re/re; rer1/RER1* and developed tiny inflorescences containing flowers with aberrant morphology (Fig. 5, B and C). They were, however, able to yield mature siliques that contained aborted ovules and embryos and exhibited asynchronous seed maturation (Fig. 5D). About 98% of the F3 seeds derived from selfed *re/re;rer1/RER1* plants displayed reticulate leaves, whereas the remaining 2% had the same severe phenotype as their parents; they were genotyped and confirmed to be *re/re;RER1/RER1* and *re/re;rer1/RER1*, respectively (Supplemental Table S3). From these results, we concluded that the *re/re; rer1/RER1* plants are escapers, because most *re;rer1* gametes are lethal, only a very low proportion of which survive past the phenocritical stage where the *RE* and *RER1* redundant functions are required.

To evaluate the redundancy of *RE* and *RER1*, we next tested whether *RER1* expression could rescue a mutant in *RE*. The expression of wild-type *RE* under the control of the 35S promoter $2x35S_{pro}$:*RE* completely rescued the reticulate leaf phenotype of *re* mutants (Fig. 5E). In addition, the $2x35S_{pro}$:*RER1* transgene partially rescued the reticulate leaf phenotype of the *re-3* mutant (Fig. 5F). Neither the $2x35S_{pro}$:*RE* nor the $2x35S_{pro}$:*RER1* transgenes altered the leaf morphologies of the wild type or the *rer1* mutants (data not shown), which indicates that an excess of RE and RER1 function is not detrimental for leaf development. Also, the phenotype of *re-3* was not modified by the functional RER3:GFP protein (Fig. 5G).

Because the expression of *RER3* in leaves fully overlaps with that of *RER1* and partially with that of *RE* (Fig. 4; see above), we combined some of their mutant alleles to study genetic interactions. The phenotypes of all the *re rer3* double mutants obtained were interpreted as additive (Supplemental Table S3), because they merely shared the morphological traits of both parentals (Fig. 5H). In the F2 generation of *rer3* × *rer1* crosses, a 3:1 (wild-type plants:reticulate plants) phenotypic segregation was obtained (Supplemental Table S2), indicating no genetic interaction. We confirmed the genotype of *rer3-3 rer1* double mutants (Fig. 5I), which were phenotypically indistinguishable from *rer3-3* (Fig. 1M). In addition, neither the $2x35S_{pro}$:*RE* nor the $2x35S_{pro}$:*RER1* transgenes rescued the reticulate leaf phenotype of *rer3* homozygotes (data not shown).

To ascertain if the *RER5* and *RER6* genes also act redundantly, we crossed the phenotypically wild-type *rer5-1* and *rer6-1* mutants (Fig. 1, I and J) and found in their F2 and F3 progeny seedlings with small rosettes, chlorotic leaves and retarded growth (Fig. 5J), whose genotype was shown to be *rer5-1/rer5-1;rer6-1/rer6-1* (Supplemental Tables S2 and S3). We then studied double mutant combinations of *rer4* and *rer6* with either *re-6* or *rer3-3*. In all cases, the double mutant plants were indistinguishable from their *re-6* or *rer3-3* parental lines (data not shown). In contrast to the results found previously for mutations affecting the same paralog pairs, *re rer1* and *rer5 rer6* (see above), we

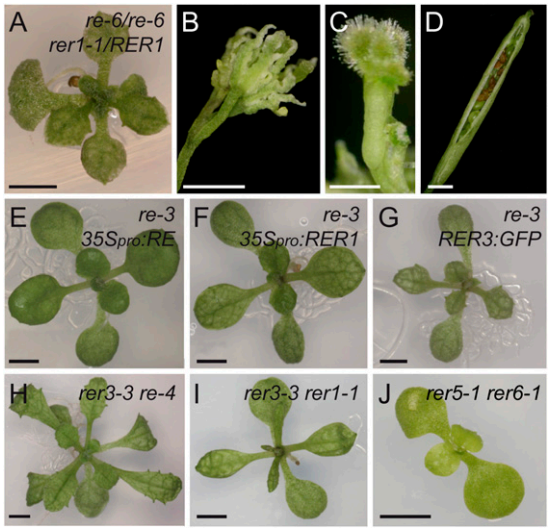

Figure 5. Genetic interactions among mutant alleles of genes of the RER family. A to D, Phenotype of rosette (A), flowers (B), and siliques of *re-6/re-6;rer1-1/RER1* (C and D). E to G, Rosettes of *re-3* expressing the $2x35S_{pro}$*:RE* (E), $2x35S_{pro}$*:RER1* (F), or $RER3_{pro}$*:RER3:GFP* (G) transgenes. H and I, Additive phenotypes of the *rer3-3 re-4* (H) and *rer3-3 rer1-1* (I) double mutants. J, Synergistic phenotype of the *rer5-1 rer6-1* double mutant. K, Additive phenotype of the *rer3-3 cue1-6* double mutant. Pictures were taken 14 (E–G, I, and J), 21 (A and H), and 45 (B–D) das. Bars = 2 mm.

found no genetic interactions between any pair of *re* and *rer* alleles from different paralog gene pairs (*re rer3*, *rer1 rer3*, *re rer4*, *rer1 rer4*, *re rer6*, *rer3 rer6*, and *rer4 rer6*; Fig. 5, H and I; Supplemental Table S2), suggesting a degree of specialization of RER function between paralogs.

The Phenotypes of the *re* and *rer3* Mutants Show Local Cell Death and Accumulation of Reactive Oxygen Species

Leaves of the *re* and *rer3* mutants contain fewer cells and larger air spaces in their palisade mesophyll than their wild types (Fig. 2). The proportions of 2C and 4C nuclei populations in the first leaf pair at 14 and 21 das were not significantly different in *re-4*, *re-6*, and *rer3-3* mutants compared with L*er* (Supplemental Table S1). These results indicate that the pool of mitotic cells were not altered by the *re* and *rer3* mutations. Hence, local cell death might account for the reticulation observed in *re* and *rer3* mutant leaves. We used trypan blue staining to examine whether mutant leaves contained dead cells. In the wild-type leaves at 14 das, we only found trypan blue staining in some elongated cells neighboring xylem vessels (Fig. 6, A and B). In the strongly reticulated *cue1-6* mutant (Fig. 1D), we found trypan blue staining accumulated around the vasculature and in some palisade mesophyll cells (Fig. 6, E and F). Similar accumulation of trypan blue was observed in the perivascular mesophyll of *re* leaves (Fig. 6, C and D). We also found increased trypan blue staining around the vasculature of *rer3* leaves (Fig. 6H) compared with both L*er* (Fig. 6G) and *rer3* $RER3_{pro}$*:RER3:GFP* plants (Fig. 6I). The proportion of nuclei debris, estimated as the nuclei population less than 2C, was slightly but significantly ($P < 0.05$) increased in *re-6* and *cue1-6* leaves (Supplemental Table S1), and additional fluorescence peaks were shown for the nuclei populations greater than 4C (data not shown), both features being indicative of nuclei with degraded DNA.

In plants, cell death can involve the accumulation of reactive oxygen species (ROS), and some of the *re* mutants were shown to overproduce ROS in their leaves (Barth and Conklin, 2003; Overmyer et al., 2008). To study the spatial distribution of ROS in *re* and *rer*, we infiltrated leaves with 3,3′-diaminobenzidine (DAB), which reacts with hydrogen peroxide (H_2O_2), allowing its visualization as a brown-colored precipitate (Vanacker et al., 2000). Enhanced H_2O_2 accumulation was confirmed in the mesophyll surrounding the vasculature of *re* and *cue1-6* leaves (Fig. 6, L and M; data not shown). Interestingly, leaves of *rer1*, which are not visibly reticulated (Fig. 1F), also exhibited DAB precipitate around the veins (Fig. 6, N and O), weaker than in the *re* mutants (Fig. 6, L and M) but stronger than in Col-0 (Fig. 6, J and K). A similar pattern of DAB precipitate in the mesophyll surrounding the vasculature was observed in *rer3* leaves (Fig. 6, R–T) but absent both in L*er* (Fig. 6, P and Q) and the transgenic plants expressing the $RER3_{pro}$*:RER3:GFP* transgene in a *rer3-3* background (Fig. 6, U and V). We confirmed that the DAB precipitates observed were specifically dependent on H_2O_2 by incubating leaves with catalase (Fig. 6, W and X).

The Phenotypes of the *re* and *rer3* Mutants Are Dependent on Light Fluency Rate and Photoperiod

Photoperiod is a major determinant of leaf development and has been shown to modulate gene expression, amino acid profiles, stomatal index, and cell death in Arabidopsis leaves (Queval et al., 2007; Lepistö et al., 2009; Chaouch et al., 2010). Analysis of photoperiod-dependent growth phenotypes revealed that the reticulate pigmentation of *re* and *rer* mutants was rescued by a short-day photoperiod (Fig. 7, A–C and I–L). The growth rate of *re-3*, *re-4*, and *rer3-3*, however, was still slower than that of their respective wild-type plants (Fig. 7, I–L). By contrast, *cue1-6* remained pale and exhibited a dwarf phenotype also under short photoperiod (Fig. 7D). Next, we explored whether photoperiod modulates the accumulation of light-induced ROS production in the *rer* mutants. The pattern of DAB staining indicated accumulation of H_2O_2 in cells surrounding the vasculature in all *re* and *rer* mutant plants grown under long photoperiod in soil (data not shown), comparable to that of the *rer* mutants grown on agar plates (Fig. 6). When grown under short photoperiod, however, neither *re*, *rer*, nor *cue1-6* mutants showed any enhancement of ROS

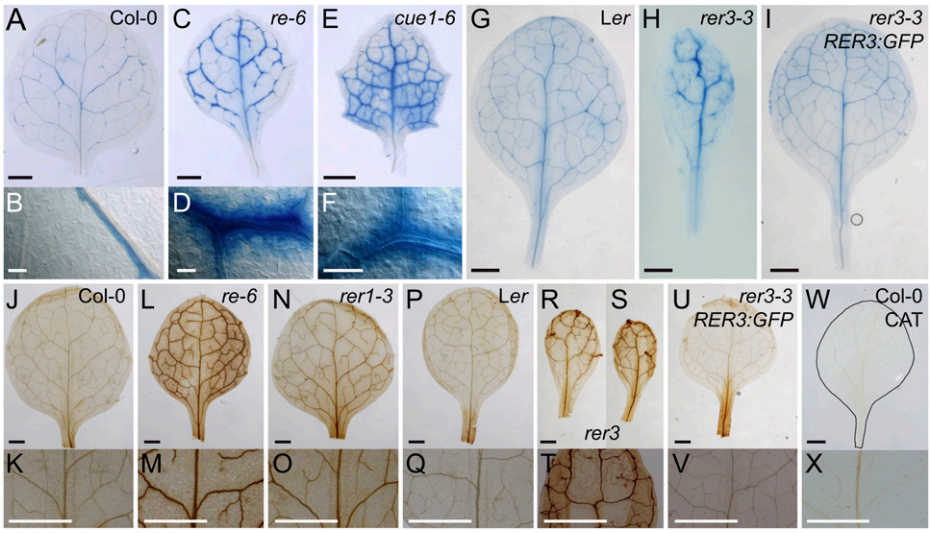

Figure 6. Cell death and ROS accumulation in leaves from mutants in RER genes. A to I, Membrane permeability for the trypan blue stain in perivascular cells from Col-0 (A and B), *re-6* (C and D), *cue1-6* (E and F), L*er* (G), *rer3-3* (H), and *rer3-3* expressing the $RER3_{pro}$:*RER3*:*GFP* transgene (I). B, D, and F, Details of trypan blue perivascular stain. J to X, H_2O_2 accumulation visualized in planta by DAB staining in Col-0 (J and K), *re-6* (L and M), *rer1-3* (N and O), L*er* (P and Q), *rer3-2* (R), *rer3-3* (S and T), *rer3-3* expressing the $RER3_{pro}$:*RER3*:*GFP* transgene (U and V), and Col-0 incubated with 100 units μL^{-1} catalase (W and X). Whole leaves (J, L, N, P, R, S, U, and W) and details of their central regions (K, M, O, Q, T, V, and X). The margin of the leaf shown in W has been highlighted by hand drawing. First- or second-node leaves were harvested 14 das. Bars = 1 mm (A, C, E, and G–X) and 50 μm (B, D, and F).

staining (Fig. 7, E–H and M–P). The photoperiod-dependent pale-green phenotypes of the *rer* mutants (Figs. 1 and 7) and the strong signal of RER3:GFP observed in small developing chloroplasts (Fig. 4) raised the question of whether RER family members are required for appropriate development of photosynthetic pigment-protein complexes. Thus, possible photoperiod-dependent adjustments in thylakoid membrane protein complexes were studied by blue-native gel electrophoresis (Supplemental Fig. S7). This revealed very similar patterns of thylakoid protein complexes in *rer* mutant and wild-type plants irrespective of the length of the photoperiod. Therefore, the basic structures of the photosynthetic machinery seem not to be drastically affected in the *re* and *rer* mutants studied.

More Than 200 Genes Are Misregulated in the *re* and *rer3* Mutants

To identify specific changes in the transcriptome of the *re* and *rer3* mutants that might account for their shared leaf reticulation phenotype, we carried out a microarray analysis using RNA extracted from *re-3* and *rer3-3* mutant rosettes (Supplemental Materials and Methods S1). We found 370 differentially expressed genes in *re-3* (137 up-regulated and 233 down-regulated genes) and 358 in *rer3-3* (173 up-regulated and 185 down-regulated), compared with L*er* (Supplemental Fig. S8A). Fifty-six percent (n = 261) of the identified genes were misregulated in both mutants, and both the sign and the magnitude of their fold change matched between the two mutants (Supplemental Table S5; $P < 0.01$). To visualize our microarray results in the context of cellular pathways and processes, we employed the MapMan tool (Thimm et al., 2004). We found a highly significant enrichment for misregulated genes belonging to the categories of "stress signaling" and "DNA" in the *re-3* and *rer3-3* mutants (Supplemental Fig. S8C). The most overrepresented Gene Ontology categories (Carbon et al., 2009) for the commonly down-regulated genes in *re-3* and *rer3-3* were those of defense response, phosphorylation, and kinase activity (Supplemental Table S5). Several genes involved in salicylic acid (SA) biosynthesis and response (*ENHANCED DISEASE SUSCEPTIBILITY1* [*EDS1*], *ARABIDOPSIS WRKY DNA-BINDING PROTEIN70* [*WRKY70*], *LATE UPREGULATED IN RESPONSE TO HYALOPERONOSPORA PARASITICA*, *ISOCHORISMATE SYNTHASE1* [*ICS1*], *ACCELERATED CELL DEATH6* [*ACD6*], *CELL WALL-ASSOCIATED KINASE1*, and *ANKYRIN*) were similarly down-regulated in both the *re* and *rer3* mutants.

To validate our microarray results, we performed quantitative RT-PCR analyses of several genes selected from the sets of up-regulated and down-regulated genes in *re-3* and *rer3-3* mutants, and in every case, the quantitative RT-PCR results matched our microarray data (Supplemental Fig. S8B).

The Metabolomes of *re* and *rer3* Mutant Leaves Share Several Alterations

Because *re* and *rer3* mutants share similar leaf phenotypes, finding metabolites whose levels are similar

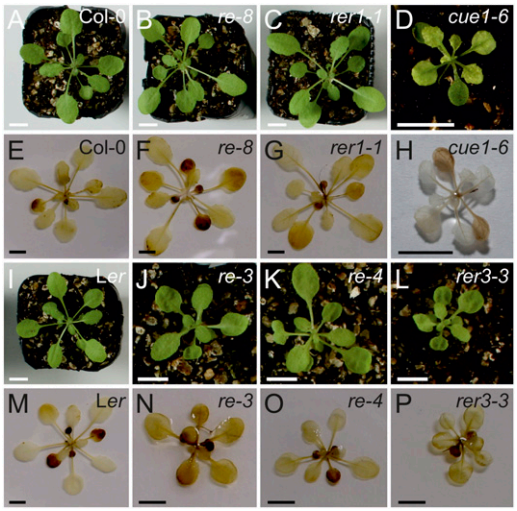

Figure 7. Photoperiod dependence of the phenotypes of mutant alleles of *CUE1* and RER family members. A to D and I to L, The reticulate phenotype of the *rer* mutants was rescued when plants were grown under short-day conditions (8 h/16 h of light/darkness). E to H and M to P, H_2O_2 accumulation in plants grown under short-day conditions visualized by DAB staining. Bars = 1 cm.

but different from the wild type could help to identify the common metabolic targets of RE and RER3 (Supplemental Fig. S9; Fig. 8). From the comparative analyses of the metabolites identified in leaves from *re-3*, *re-4*, and *rer3-3* mutants and those of their wild-type L*er*, we spotted 63 metabolites whose levels differed significantly (or highly significantly) between the mutants and the wild type (Supplemental Fig. S9; Supplemental Table S6). Metabolite accumulation in *re-3* and *re-4* mutants was highly similar (data not shown), as expected for two alleles that similarly affect *RE* function. Interestingly, 14 metabolites showed similar accumulation profiles in all three mutants, with 11 that were decreased and three that were increased in the mutants compared with the wild type (Supplemental Table S6). We observed a decrease in the levels of the branched amino acids Ile and Val and the aromatic amino acids Tyr, Phe, and Trp, as well as Ala and Met in *re* and *rer3* mutant leaves (Fig. 8; Supplemental Table S6). In addition, the *re* and *rer3* mutants also displayed a reduction of shikimate and of the downstream products of its pathway, such as aromatic amino acids (see above), cinnamic acid, sinapate, and indole-3-acetonitrile (Fig. 8; Supplemental Table S6). PEP is used as a substrate in the shikimate pathway for the biosynthesis of aromatic amino acids and in the tricarboxylic acid (TCA) cycle (Li et al., 1995; Streatfield et al., 1999; Knappe et al., 2003; Voll et al., 2003). The TCA cycle intermediates succinate, fumarate, and malate were decreased in the *re* and *rer3* mutants compared with the wild type. In addition, the *re* and *rer3* mutants contain lower levels of pyruvate (Fig. 8; Supplemental Table S6). In conclusion, the metabolic profiles of mature leaves in *re* and *rer3* mutants revealed that several biosynthetic pathways downstream of PEP are altered in the mutants.

RE and *RER3* Do Not Genetically Interact with *VEN3*, *VEN6*, *NOA1*, *AS1*, or *AS2*

To determine whether other reticulate mutants might function by common mechanisms, we also looked for a potential genetic interaction with *re* or *rer3*. The leaves of *ven3* and *ven6* semidominant mutants, whose wild-type alleles encode the subunits of the CPS required for the conversion of Orn into citrulline in the Arg biosynthesis pathway (Mollá-Morales et al., 2011), display green primary and secondary veins with a paler lamina (Supplemental Fig. S10A). Leaf reticulation in the *ven3* and *ven6* mutants can be fully rescued by exogenously applied citrulline, but Orn reduces overall growth of these two mutants further than in their wild-type L*er* (Mollá-Morales et al., 2011). We found that *re* and *rer3* seedlings display a similar growth reduction to L*er* on Orn-supplemented plates (data not shown). By contrast, all the *re*, but not *rer*, mutants studied displayed severe growth retardation and enhanced leaf reticulation when grown on citrulline-supplemented plates, regardless of their L*er* or Col-0 genetic background (data not shown). Consistent with these results, all the double mutant combinations of *ven3* or *ven6* with *re* or *rer3* caused additive leaf phenotypes (Supplemental Fig. S10, E and I; Supplemental Tables S2 and S3). NITRIC OXIDE ASSOCIATED1 (NOA1; Flores-Pérez et al., 2008) is required for chloroplast photosynthetic function (Van Ree et al., 2011). The *noa1-2* null allele, which causes pale-green leaves (Supplemental Fig. S10B), additively interacts with *re-4* and *rer3-2* (Supplemental Fig. S10, F and J; Supplemental Tables S2 and S3).

Mutant alleles of genes encoding ribosomal proteins cause leaf reticulation and synergistically interact with alleles of *ASYMMETRIC LEAVES1* (*AS1*; Supplemental Fig. S10C) or *AS2* (Supplemental Fig. S10D) genes (Horiguchi et al., 2011). We wondered whether an overall reduction in the cell numbers in the mesophyll, as observed in *re* and *rer3* mutant leaves, would constitutively enhance the leaf polarity defects caused by the *as1* and *as2* mutations and produce radialized leaves (Szakonyi et al., 2010). However, all the double mutants obtained involving *as1* or *as2* with *re* or *rer3* alleles displayed an additive leaf phenotype consisting of asymmetric and reticulate leaves (Supplemental Fig. S10, G, H, K, and L; Supplemental Tables S2 and S3). Hence, an overall reduction of palisade mesophyll cell numbers is not sufficient to enhance the *as1* and *as2* leaf phenotypes. Given than an additive double mutant phenotype is widely accepted as a sign of absence of a functional relationship between the mutated genes under study (Pérez-Pérez et al., 2009), our results indicate that the functions of RE and RER3 are not related to those of VEN3, VEN6, NOA1, AS1, or AS2.

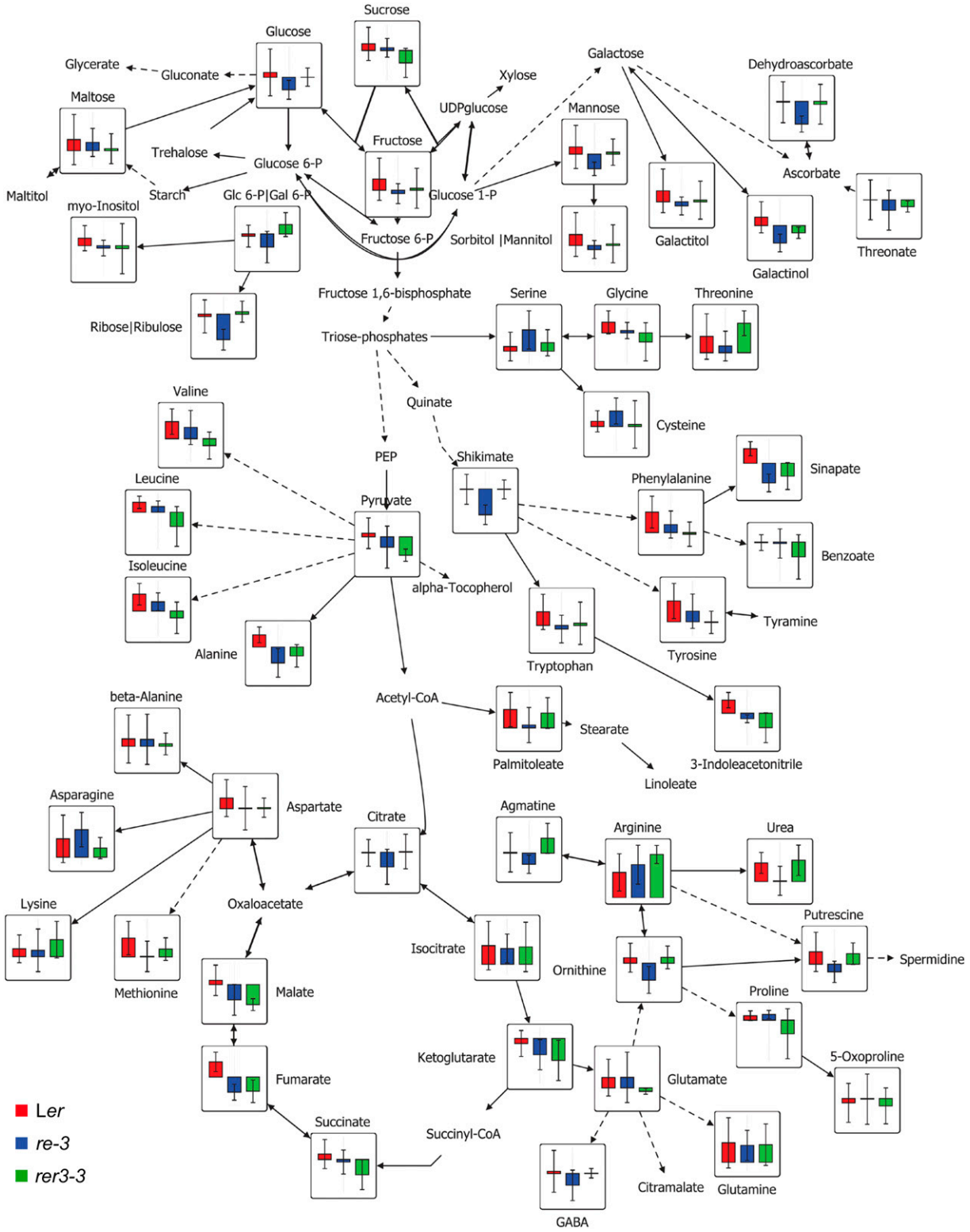

Figure 8. Changes of metabolite responses in L*er*, *re-3*, and *rer3-3* leaves. Each node represents a metabolite, connected by solid and dashed lines that represent single and lumped enzyme reactions, respectively. Data are means of eight independent samples. Significant changes were evaluated by Student's *t* test ($P < 0.05$). The map was created using the VANTED software (version 1.66).

DISCUSSION

Members of the RER Family Can Be Classified into Four Functional Modules

The plant-specific RER proteins are integral components of the chloroplast envelope membranes (RE, RER1, RER3, and RER4) and the thylakoids (RER5 and RER6; Ferro et al., 2003, 2010; Froehlich et al., 2003; Kleffmann et al., 2004; Dunkley et al., 2006; Zybailov et al., 2008). Based on protein similarity, gene expression, and loss- and gain-of-function studies, we identified four functional modules for the RER family, three of which include pairs of close paralogs (*RE* and *RER1*, *RER2* and *RER3*, and *RER5* and *RER6*). The expression of *RE*, *RER1*, and *RER3* overlaps in the bundle sheath cells of mature leaves and roots, but it is region specific and gene specific in young and developing organs. We determined that *RE* and *RER1* perform unequal but redundant functions in palisade mesophyll development and are essential for the haploid stage of the life cycle of the plant. By contrast, *RER5* and *RER6* are functionally redundant during leaf growth, as indicated by the synergistic phenotype of the *rer5-1 rer6-1* double mutants. In addition, the additive mutant phenotypes obtained when combining two mutations, each affecting genes of different modules, is consistent with the four functional modules we defined within the RER family.

Among the *RER* genes, we can postulate a specific function for *RER3* during embryogenesis related to auxin signaling, based on the embryonic phenotype and *DR5rev*:*GFP* expression in the *rer3* mutants. The defects caused by *rer3* alleles during embryogenesis are reminiscent of those observed in auxin-signaling mutants, such as *monopteros* (Hardtke and Berleth, 1998), *bodenlos* (Hamann et al., 1999), and *pin-formed1* (Aida et al., 2002). Auxin signaling, as measured by *DR5rev*:*GFP*, was enhanced in *rer3* mutants, similar to some auxin-signaling mutants (Pérez-Pérez et al., 2010). Interestingly, mutations in *ANTHRANILATE SYNTHASE1*, encoding the key enzyme of Trp biosynthesis, an auxin precursor (Niyogi and Fink, 1992), were found to synergistically enhance the embryonic phenotype of *rer3* homozygotes (J.M. Pérez-Pérez, A. Mollá-Morales, and J.L. Micol, unpublished data). Further experiments are ongoing in our laboratory to assess whether RER3 function is specifically required in the auxin biosynthesis pathway as suggested by these results.

Several Pathways Downstream of PEP Are Altered in the *re* and *rer3* Mutants

The *re* and *rer3* mutant leaves contain low levels of pyruvate and downstream products of PEP, such as aromatic amino acids and fumarate, which are a major storage form of fixed carbon in Arabidopsis (Chia et al., 2000). Lehmann et al. (2009) suggested that those changes could be attributed to oxidative inhibition of the TCA cycle and the subsequent slowdown of linked amino acid biosynthesis pathways. Alternatively, a defective photosynthetic function, due to the overall reduction of palisade mesophyll cells observed in *re* and *rer3* mutants, may underlie the reduced fumarate accumulation that we observed in mutant leaves. Some glycolysis and TCA cycle intermediates are subsequently used as substrates for numerous metabolic pathways, most of which take place in the chloroplasts. In fact, similarities in the levels of other metabolites from the shikimate pathway, namely shikimate, aromatic amino acids, sinapate, and indol-3-eacetonitrile, were observed in *re* and *rer3* mutants, indicating some conservation of the basic regulatory response. The synergistic phenotype of the few *re/re;rer1/RER1* escapers resembled that of the reticulated *cue1* mutant, which exhibits impaired activity of a PEP/phosphate translocator strongly expressed in bundle sheath cells of developing leaves (Li et al., 1995; Streatfield et al., 1999). Even though the molecular function of RER family members remains to be established, it is striking that mutations in *CUE1*, *RE*, and *RER3* cause an imbalance in the shikimate pathway and the downstream biosynthesis of aromatic amino acids in chloroplasts and have similar long-range effects on the development of mesophyll tissue in leaves (Knappe et al., 2003; Voll et al., 2003). One intriguing possibility is that some RER proteins modulate the activity of the CUE1 transporter at the chloroplast inner membrane; however, our attempts to coimmunoprecipitate the CUE1 protein with RER3 in plants expressing the $RER3_{pro}$:*RER3*:*GFP* transgene were unsuccessful (R. González-Bayón, M.R. Ponce, and J.L. Micol, unpublished data).

The *re* and *rer3* mutants also showed down-regulation of genes encoding receptor kinases, calcium signaling components, and genes involved in the primary response to pathogens. These findings indicate that the increased susceptibility to *Pseudomonas syringae* previously observed for other *re* alleles (Barth and Conklin, 2003) is not a consequence of decreased cellular density per se. Rather, reduced expression of *ICS1*, encoding the rate-limiting enzyme in SA biosynthesis (Wildermuth et al., 2001), as well as of *EDS1* (Vanderauwera et al., 2011), *WRKY70* (Ulker et al., 2007), and *ACD6* (Lu et al., 2003), which encode key components of SA signaling, suggest specific deficiencies in SA-dependent defense responses in *re* and *rer3* mutants (González-Bayón et al., 2006). The biosynthesis of SA takes place in the chloroplasts and is derived from the Trp branch of the shikimate pathway (Métraux, 2002), which was found to be altered in the *re* and *rer3* mutants. In addition to the downstream effects on SA biosynthesis, the impact of foliar amino acid contents on plant disease resistance has recently become evident (Liu et al., 2010). Such metabolic cross talk is highly sensitive to interorganellar communication, and a key role for the chloroplast envelope in cellular signaling and the maintenance of metabolic homeostasis between different cellular compartments has been recently proposed (Furumoto et al., 2011; Sun et al., 2011).

Reticulation and Accumulation of ROS Are Associated in *re* and *rer* Mutant Leaves

Leaf reticulation has been hypothesized to result from the loss of function of one or more genetic modules required for the development of mesophyll cells (González-Bayón et al., 2006; Mollá-Morales et al., 2011). Strikingly, all functionally characterized reticulated mutants are affected in primary metabolic genes and consequently in primary metabolism (Streatfield et al., 1999; Mollá-Morales et al., 2011; Rosar et al., 2012). Because the differentiation of bundle sheath cells precedes mesophyll differentiation (Kinsman and Pyke, 1998), a limited supply of essential metabolites might only become damaging for mesophyll cells over the long term. Consistent with this hypothesis, malate levels were decreased in *re* and *rer3* mutants, which might become limiting for photosynthesis of mesophyll cells located further away from the xylem, as malate is being transported from the roots to fuel photosynthesis (Hibberd and Quick, 2002). Alternatively, the gene function might be equally important in mesophyll and bundle sheath cells; however, if the gene is highly expressed in bundle sheath cells, a partial loss of function will not become limiting for the latter. Those bundle sheath cells, which differentiate before deficiencies become damaging, later experience long-term consequences, such as enhanced oxidative stress. As a result, the symptoms of damage are observed in mature bundle sheath cells, even though the greatest defects occurred earlier during mesophyll development. Also, we have established that the phenotype caused by the chemical inhibition of chloroplast differentiation was epistatic over the reticulate leaf phenotype of *re* and *rer3* mutants, suggesting that the pathway altered in these mutants leading to leaf reticulation is downstream of chloroplast differentiation.

As determined by ploidy analysis, the reduced number of palisade mesophyll cells in *re* and *rer3* might arise from enhanced cell death, and not from altered cell proliferation, as previously suggested (González-Bayón et al., 2006). What causes the death of mesophyll cells in *re* and *rer* mutants? Associated with the reticulated pigmentation, a long photoperiod determines ROS accumulation in the leaves of all the *re* and *rer* mutants studied. Metabolite profile analysis of *re* and *rer3* mutants revealed a decrease in levels of dehydroascorbate, the reduced form of ascorbate that protects plants against free radicals and oxidative stress (Horemans et al., 2000). Down-regulation of TCA intermediates has been reported in response to oxidative stress (Obata et al., 2011). Moreover, elevated ROS levels are accompanied by ectopic cell death in perivascular leaf tissues in mature *re* and *rer* mutant leaves, as measured by increased permeability to trypan blue. In addition, leaf reticulation of *re* and *rer3* leaves is suppressed under a short-day photoperiod, a condition that limits light-induced ROS production. However, whether this suppression is determined by the severity or the duration of light-induced ROS production remains to be determined. If the phenotype is photoperiod dependent, as observed for *catalase2*-deficient mutants (Queval et al., 2007), this will provide an interesting additional link between ROS signaling and daylength. A connection between reduced ploidy level, ROS accumulation, and initiation of cell death is further supported by increased abundance of transcripts for cell cycle checkpoint genes (*ARABIDOPSIS BREAST CANCER SUSCEPTIBILITY1*, *CYCLIN B1;1*, and *UV REPAIR DEFECTIVE3*) in *re* and *rer3* leaves. Vanderauwera et al. (2011) proposed that ROS produced in specific cellular compartments may trigger the DNA damage response, whereby activation of cell cycle checkpoint genes may be essential for protection against cell death under photooxidative stress.

MATERIALS AND METHODS

Plant Material and Growth Conditions

Arabidopsis (*Arabidopsis thaliana*) *ven5-1*, *ven5-2*, and *ven5-3* mutants were isolated as described in Berná et al. (1999). T-DNA insertion lines (Table I) were obtained from the Nottingham Arabidopsis Stock Centre (http://arabidopsis.info/) and are described at the SIGnAL Web site (http://signal.salk.edu/). We confirmed the T-DNA insertion sites of all the mutant lines by PCR amplification using the gene-specific primer pairs and the left border primers of the T-DNA insertion listed in Supplemental Table S4.

All plants studied in this work are homozygous for the mutations indicated unless otherwise stated. Plants were grown under sterile conditions on 150-mm petri dishes, each containing 100 mL of one-half-strength Murashige and Skoog agar medium with 1% (w/v) Suc at 20°C ± 1°C, 60% to 70% relative humidity, and continuous illumination at 80 μmol m^{-2} s^{-1}, as described in Ponce et al. (1998). Treatment of mutant and wild-type seedlings with exogenous Arg biosynthesis intermediates (Mollá-Morales et al., 2011) was performed as described elsewhere.

For analyses under different photoperiods, wild-type and mutant plants were grown in a mixture of vermiculite and soil (1:1) under 130 μmol m^{-2} s^{-1} at 22°C, 50% relative humidity, and under short-day (8 h/16 h of light/darkness) or long-day (16 h/8 h of light/darkness) conditions.

In Silico Analyses

Homologous RER proteins were identified from public databases using the Paralog Search Tool at the KEGG Sequence Similarity DataBase (Masoudi-Nejad et al., 2007). The neighbor-joining tree of RER proteins was constructed with MEGA5.1 (Tamura et al., 2011). Information on the subcellular localization of the RER proteins was retrieved from the Arabidopsis Subcellular Database (Heazlewood et al., 2007). Predicted transmembrane domains were obtained from the ARAMEMNON database (Schwacke et al., 2003). Analysis of protein domains was performed using SMART (Letunic et al., 2009), and chloroplast transit peptides were predicted with ChloroP 1.1 (Emanuelsson et al., 1999). Expression data for genes of the RER family was retrieved from the Arabidopsis eFP browser (Schmid et al., 2005; Winter et al., 2007) and the ATTED-II database (Obayashi et al., 2009).

Gene Constructs and Plant Transformation

For promoter-reporter gene transcriptional fusions (RE_{pro}:*GUS*, $RER1_{pro}$:*GUS*, and $RER3_{pro}$:*GUS*), 2.2-, 2.1-, and 1.6-kb segments of the regions upstream to the *RE*, *RER1*, and *RER3* transcription units were PCR amplified from wild-type Col-0 genomic DNA with PfuUltra (Agilent Technologies), using the primers listed in Supplemental Table S4. PCR products were purified with the Illustra GFX PCR DNA and Gel Band Purification Kit (GE Healthcare Life Sciences) and cloned into the pENTR/D-TOPO vector (Life Technologies) following the manufacturer's instructions. Chemically competent *Escherichia coli* DH5α cells were heat shocked, and the putative transformants were confirmed for insert orientation and structural integrity by PCR and sequencing. The target sequences were subcloned via an LR Clonase II (Life Technologies) reaction into the pMDC162 Gateway-compatible vector containing the *gusA* gene, which encodes the GUS enzyme (Curtis and

Grossniklaus, 2003). For constitutive expression constructs (*2x35S$_{pro}$:RE* and *2x35S$_{pro}$:RER1*), 2.5- and 3.0-kb fragments of genomic DNA including the entire coding region of *RE* and *RER1* were amplified and cloned into the pENTR/D-TOPO as described above and then subcloned into the pMDC32 plasmid, harboring two copies of the *Cauliflower mosaic virus* 35S promoter (Curtis and Grossniklaus, 2003), using Gateway technology (Life Technologies). The *RER3$_{pro}$:RER3:GFP* translational fusion, under the control of the endogenous *RER3* promoter, was obtained from a 2.7-kb PCR product amplified from wild-type genomic DNA with the pRER3-F and gRER3-R primers (Supplemental Table S4), cloned into pENTR/D-TOPO, and then subcloned in pMDC107 (Curtis and Grossniklaus, 2003), as described above.

All the above-mentioned constructs were mobilized into *Agrobacterium tumefaciens* GV3101 (C58C1 Rif^R) cells and further transferred into Col-0 or *rer3-3* plants by the floral dip method (Clough and Bent, 1998). T1 transgenic plants were selected on plates supplemented with 15 μg mL^{-1} hygromycin under our standard sterile culture conditions. Several T2 lines were selected for characterization. GUS staining was performed on homozygous T2 and T3 plants as previously described (Pérez-Pérez et al., 2010).

Morphological and Histological Analyses

To study seedling and root morphologies, at least 30 plants per genotype were grown in vertically oriented agar plates, and their seedling and root phenotypes were scored at 7, 9, and 12 das. Lengths of at least 15 roots were measured at 9 das, and Mann-Whitney *U* tests were performed with the Statistical Package for the Social Sciences 16.0.2 software. For embryo visualization, fertilized siliques from 6-week-old plants were manually excised, and their seeds were mounted in a 2:1:1 mix of chloral hydrate:glycerol:water and observed by DIC microscopy as previously described (Willemsen et al., 1998).

Rosette and leaf pictures were taken 14 and 21 das with a Panasonic DMC-FX9 digital camera (2,816 × 2,112 pixels). Individual rosette information was extracted from these pictures using the NIS Elements AR 2.30 image analysis package (Nikon). Leaf clearing, fixation, and embedding, as well as observation of tissues by confocal microscopy, were performed as previously described (Candela et al., 1999; González-Bayón et al., 2006). Chlorophyll solubilization was completed by incubating the excised leaves on a methanol:acetone mixture for 30 min at –20°C and then transferring the samples to phosphate buffer, pH 6.8, prior to confocal microscopy. Adaxial epidermis diagrams were obtained by drawing cell outlines on the screen of a Wacom Cintiq 18SX Interactive Pen Display (Wacom Company) using the Adobe Photoshop CS3 program. Micrographs of whole leaves and leaf sections were taken as previously described (Serrano-Cartagena et al., 2000; Pérez-Pérez et al., 2002).

Cell Death and ROS Assays

In leaf tissues, dying cells were visualized by lactophenol-trypan blue staining as described in Pavet et al. (2005). For DAB staining, 14 das, leaves were excised and immersed in a 1% (w/v) solution of DAB in Tris-HCl buffer, pH 4.8. After vacuum infiltration (30 min), the leaf samples were incubated for 8 h in darkness and then fixed in 96% (v/v) ethanol and cleared with a chloral hydrate solution (80 g chloral hydrate in 30 mL distilled water) before observation by microscopy. To confirm the specific accumulation of H_2O_2, we incubated leaves with or without 100 units μL^{-1} catalase (Sigma-Aldrich) for 30 min and processed thereafter as indicated above but with longer vacuum infiltration (120 min).

To determine the photoperiod dependency of ROS accumulation, rosettes grown in long- or short-day conditions were excised at the end of the light period and incubated overnight in darkness on petri dishes containing a 0.1 mg mL^{-1} solution of DAB, pH 7.0. At the onset of the light period, the dishes were transferred to light (130 μmol m^{-2} s^{-1} at 22°C) for 2 h. Thereafter, the rosettes were incubated in 96% (v/v) ethanol until chlorophyll was bleached and finally photographed under a Zeiss Lumar V12 stereomicroscope.

Metabolite Determination

For metabolite determination, eight biological replicates were obtained from L*er*, *re-3*, *re-4*, and *rer3-3*, with each replicate consisting of a pool of third- and fourth-node leaf laminae from 21-d-old plants grown on one-half-strength Murashige and Skoog plates at a density of 40 seedlings per plate under our standard sterile culture conditions. Samples were immediately frozen in liquid nitrogen for storage. Extraction and derivatization of metabolites from leaves using gas chromatography-mass spectrometry (GC-MS) were performed as outlined by Lisec et al. (2006) in at least four replicates. GC-MS data were obtained using an Agilent 7683 series autosampler coupled to an Agilent 6890 gas chromatograph and a Leco Pegasus 2 time-of-flight mass spectrometer. Chromatogram acquisition parameters were identical to those previously described (Weckwerth et al., 2004). Chromatograms were exported from Leco ChromaTOF software (version 3.25) to R software (http://www.r-project.org/). Peak detection, retention time alignment, and library matching were obtained using the TargetSearch package from Bioconductor (Cuadros-Inostroza et al., 2009). Metabolites were quantified by the peak intensity of a selective mass. Metabolite intensities were normalized to the fresh weight and the internal standard (C^{13} sorbitol). In addition, completely randomized GC-MS samples were measured on two consecutive days and normalized for the measurement-day effect by dividing each metabolite value by the median of all values for this metabolite measured in the same batch followed by a $\log_2$ transformation to center the values around zero (Lisec et al., 2006). The median from at least four biological replicates per genotype was determined for each of the 63 metabolites. The significance of metabolites was tested by comparing all mutants against their respective wild types ($P < 0.05$), followed by false discovery rate correction (FDR < 0.05). Heat maps and box plots were generated using R software. Principal component analysis was performed using the pcaMethods bioconductor package (Stacklies et al., 2007). Metabolite data were mapped into a schematic pathway using VANTED version 1.66 software (Junker et al., 2006).

Supplemental Data

The following materials are available in the online version of this article.

Supplemental Figure S1. Alignment of the amino acid sequences of proteins of the Arabidopsis RER family.

Supplemental Figure S2. *RER* expression in the T-DNA insertional mutants studied in this work.

Supplemental Figure S3. *DR5rev:GFP* expression in *re* and *rer3* mutants.

Supplemental Figure S4. In silico expression profiles of genes of the RER family.

Supplemental Figure S5. Coexpressed gene networks of RER family members.

Supplemental Figure S6. Expression of genes of the RER family in roots, flowers, and embryos.

Supplemental Figure S7. Thylakoid membrane protein complexes in *re*, *rer1*, *rer3*, and *cue1* mutants.

Supplemental Figure S8. Gene expression profiling in the *re-3* and *rer3-3* mutants.

Supplemental Figure S9. Overview of metabolite responses in the *re-3* and *rer3-3* mutants.

Supplemental Figure S10. Genetic interactions involving reticulate and other leaf mutants.

Supplemental Table S1. Nuclear DNA ploidy distribution in the first pair of leaves of the *re* and *rer3* mutants.

Supplemental Table S2. Phenotypic segregation in the F2 of crosses performed to study genetic interactions.

Supplemental Table S3. Phenotypic segregation in the F3 of crosses performed to study genetic interactions.

Supplemental Table S4. Primers used in this work.

Supplemental Table S5. Microarray analysis of *re-3* and *rer3-3*.

Supplemental Table S6. Metabolite profiling of *re-3* and *rer3-3*.

Supplemental Materials and Methods S1.

ACKNOWLEDGMENTS

We thank José León (Instituto de Biología Molecular y Celular de Plantas, Valencia, Spain) for the *noa1-2* seeds and Francisca M. Lozano, José M. Serrano, Tania Trujillo, Diana Navarro, and Leila Serna (Instituto de Bioingeniería,

Universidad Miguel Hernández), and Janina Stauffer and Moona Rahikainen (Department of Biochemistry and Food Chemistry, University of Turku) for technical help.

Received March 6, 2013; accepted April 17, 2013; published April 17, 2013.

LITERATURE CITED

Aida M, Vernoux T, Furutani M, Traas J, Tasaka M (2002) Roles of *PIN-FORMED1* and *MONOPTEROS* in pattern formation of the apical region of the *Arabidopsis* embryo. Development **129:** 3965–3974

Alonso JM, Stepanova AN, Leisse TJ, Kim CJ, Chen H, Shinn P, Stevenson DK, Zimmerman J, Barajas P, Cheuk R, et al (2003) Genome-wide insertional mutagenesis of *Arabidopsis thaliana*. Science **301:** 653–657

Barth C, Conklin PL (2003) The lower cell density of leaf parenchyma in the *Arabidopsis thaliana* mutant *lcd1-1* is associated with increased sensitivity to ozone and virulent *Pseudomonas syringae*. Plant J **35:** 206–218

Benková E, Michniewicz M, Sauer M, Teichmann T, Seifertová D, Jürgens G, Friml J (2003) Local, efflux-dependent auxin gradients as a common module for plant organ formation. Cell **115:** 591–602

Berná G, Robles P, Micol JL (1999) A mutational analysis of leaf morphogenesis in *Arabidopsis thaliana*. Genetics **152:** 729–742

Candela H, Martínez-Laborda A, Micol JL (1999) Venation pattern formation in *Arabidopsis thaliana* vegetative leaves. Dev Biol **205:** 205–216

Carbon S, Ireland A, Mungall CJ, Shu S, Marshall B, Lewis S (2009) AmiGO: online access to ontology and annotation data. Bioinformatics **25:** 288–289

Clough SJ, Bent AF (1998) Floral dip: a simplified method for *Agrobacterium*-mediated transformation of *Arabidopsis thaliana*. Plant J **16:** 735–743

Cuadros-Inostroza A, Caldana C, Redestig H, Kusano M, Lisec J, Peña-Cortés H, Willmitzer L, Hannah MA (2009) TargetSearch - a Bioconductor package for the efficient preprocessing of GC-MS metabolite profiling data. BMC Bioinformatics **10:** 12

Curtis MD, Grossniklaus U (2003) A gateway cloning vector set for high-throughput functional analysis of genes in planta. Plant Physiol **133:** 462–469

Chaouch S, Queval G, Vanderauwera S, Mhamdi A, Vandorpe M, Langlois-Meurinne M, Van Breusegem F, Saindrenan P, Noctor G (2010) Peroxisomal hydrogen peroxide is coupled to biotic defense responses by ISOCHORISMATE SYNTHASE1 in a daylength-related manner. Plant Physiol **153:** 1692–1705

Chia DW, Yoder TJ, Reiter WD, Gibson SI (2000) Fumaric acid: an overlooked form of fixed carbon in *Arabidopsis* and other plant species. Planta **211:** 743–751

Dunkley TP, Hester S, Shadforth IP, Runions J, Weimar T, Hanton SL, Griffin JL, Bessant C, Brandizzi F, Hawes C, et al (2006) Mapping the *Arabidopsis* organelle proteome. Proc Natl Acad Sci USA **103:** 6518–6523

Emanuelsson O, Nielsen H, von Heijne G (1999) ChloroP, a neural network-based method for predicting chloroplast transit peptides and their cleavage sites. Protein Sci **8:** 978–984

Fernández AP, Strand A (2008) Retrograde signaling and plant stress: plastid signals initiate cellular stress responses. Curr Opin Plant Biol **11:** 509–513

Ferro M, Brugière S, Salvi D, Seigneurin-Berny D, Court M, Moyet L, Ramus C, Miras S, Mellal M, Le Gall S, et al (2010) AT_CHLORO, a comprehensive chloroplast proteome database with subplastidial localization and curated information on envelope proteins. Mol Cell Proteomics **9:** 1063–1084

Ferro M, Salvi D, Brugière S, Miras S, Kowalski S, Louwagie M, Garin J, Joyard J, Rolland N (2003) Proteomics of the chloroplast envelope membranes from *Arabidopsis thaliana*. Mol Cell Proteomics **2:** 325–345

Fischer K, Kammerer B, Gutensohn M, Arbinger B, Weber A, Häusler RE, Flügge UI (1997) A new class of plastidic phosphate translocators: a putative link between primary and secondary metabolism by the phosphoenolpyruvate/phosphate antiporter. Plant Cell **9:** 453–462

Flores-Pérez U, Sauret-Güeto S, Gas E, Jarvis P, Rodríguez-Concepción M (2008) A mutant impaired in the production of plastome-encoded proteins uncovers a mechanism for the homeostasis of isoprenoid biosynthetic enzymes in *Arabidopsis* plastids. Plant Cell **20:** 1303–1315

Friso G, Majeran W, Huang M, Sun Q, van Wijk KJ (2010) Reconstruction of metabolic pathways, protein expression, and homeostasis machineries across maize bundle sheath and mesophyll chloroplasts: large-scale quantitative proteomics using the first maize genome assembly. Plant Physiol **152:** 1219–1250

Froehlich JE, Wilkerson CG, Ray WK, McAndrew RS, Osteryoung KW, Gage DA, Phinney BS (2003) Proteomic study of the *Arabidopsis thaliana* chloroplastic envelope membrane utilizing alternatives to traditional two-dimensional electrophoresis. J Proteome Res **2:** 413–425

Furumoto T, Yamaguchi T, Ohshima-Ichie Y, Nakamura M, Tsuchida-Iwata Y, Shimamura M, Ohnishi J, Hata S, Gowik U, Westhoff P, et al (2011) A plastidial sodium-dependent pyruvate transporter. Nature **476:** 472–475

González-Bayón R, Kinsman EA, Quesada V, Vera A, Robles P, Ponce MR, Pyke KA, Micol JL (2006) Mutations in the *RETICULATA* gene dramatically alter internal architecture but have little effect on overall organ shape in *Arabidopsis* leaves. J Exp Bot **57:** 3019–3031

Hamann T, Mayer U, Jürgens G (1999) The auxin-insensitive *bodenlos* mutation affects primary root formation and apical-basal patterning in the *Arabidopsis* embryo. Development **126:** 1387–1395

Hardtke CS, Berleth T (1998) The *Arabidopsis* gene *MONOPTEROS* encodes a transcription factor mediating embryo axis formation and vascular development. EMBO J **17:** 1405–1411

Heazlewood JL, Verboom RE, Tonti-Filippini J, Small I, Millar AH (2007) SUBA: the Arabidopsis subcellular database. Nucleic Acids Res **35:** D213–D218

Hibberd JM, Quick WP (2002) Characteristics of C_4 photosynthesis in stems and petioles of C_3 flowering plants. Nature **415:** 451–454

Horemans N, Foyer CH, Asard H (2000) Transport and action of ascorbate at the plant plasma membrane. Trends Plant Sci **5:** 263–267

Horiguchi G, Mollá-Morales A, Pérez-Pérez JM, Kojima K, Robles P, Ponce MR, Micol JL, Tsukaya H (2011) Differential contributions of ribosomal protein genes to *Arabidopsis thaliana* leaf development. Plant J **65:** 724–736

Janacek SH, Trenkamp S, Palmer B, Brown NJ, Parsley K, Stanley S, Astley HM, Rolfe SA, Paul Quick W, Fernie AR, et al (2009) Photosynthesis in cells around veins of the $C_{(3)}$ plant *Arabidopsis thaliana* is important for both the shikimate pathway and leaf senescence as well as contributing to plant fitness. Plant J **59:** 329–343

Junker BH, Klukas C, Schreiber F (2006) VANTED: a system for advanced data analysis and visualization in the context of biological networks. BMC Bioinformatics **7:** 109

Kinsman EA, Pyke KA (1998) Bundle sheath cells and cell-specific plastid development in *Arabidopsis* leaves. Development **125:** 1815–1822

Kleffmann T, Russenberger D, von Zychlinski A, Christopher W, Sjölander K, Gruissem W, Baginsky S (2004) The *Arabidopsis thaliana* chloroplast proteome reveals pathway abundance and novel protein functions. Curr Biol **14:** 354–362

Knappe S, Löttgert T, Schneider A, Voll L, Flügge UI, Fischer K (2003) Characterization of two functional *phosphoenolpyruvate/phosphate translocator* (*PPT*) genes in *Arabidopsis*—*AtPPT1* may be involved in the provision of signals for correct mesophyll development. Plant J **36:** 411–420

Leegood RC (2008) Roles of the bundle sheath cells in leaves of C_3 plants. J Exp Bot **59:** 1663–1673

Lehmann M, Schwarzländer M, Obata T, Sirikantaramas S, Burow M, Olsen CE, Tohge T, Fricker MD, Møller BL, Fernie AR, et al (2009) The metabolic response of *Arabidopsis* roots to oxidative stress is distinct from that of heterotrophic cells in culture and highlights a complex relationship between the levels of transcripts, metabolites, and flux. Mol Plant **2:** 390–406

Lepistö A, Kangasjärvi S, Luomala EM, Brader G, Sipari N, Keränen M, Keinänen M, Rintamäki E (2009) Chloroplast NADPH-thioredoxin reductase interacts with photoperiodic development in Arabidopsis. Plant Physiol **149:** 1261–1276

Letunic I, Doerks T, Bork P (2009) SMART 6: recent updates and new developments. Nucleic Acids Res **37:** D229–D232

Li H, Culligan K, Dixon RA, Chory J (1995) *CUE1*: a mesophyll cell-specific positive regulator of light-controlled gene expression in *Arabidopsis*. Plant Cell **7:** 1599–1610

Li Y, Rosso MG, Viehoever P, Weisshaar B (2007) GABI-Kat SimpleSearch: an *Arabidopsis thaliana* T-DNA mutant database with detailed information for confirmed insertions. Nucleic Acids Res **35:** D874–D878

Lisec J, Schauer N, Kopka J, Willmitzer L, Fernie AR (2006) Gas chromatography mass spectrometry-based metabolite profiling in plants. Nat Protoc **1:** 387–396

Liu X, Rodermel SR, Yu F (2010) A *var2* leaf variegation suppressor locus, *SUPPRESSOR OF VARIEGATION3*, encodes a putative chloroplast

translation elongation factor that is important for chloroplast development in the cold. BMC Plant Biol **10:** 287

Lu H, Rate DN, Song JT, Greenberg JT (2003) ACD6, a novel ankyrin protein, is a regulator and an effector of salicylic acid signaling in the *Arabidopsis* defense response. Plant Cell **15:** 2408–2420

Masoudi-Nejad A, Goto S, Endo TR, Kanehisa M (2007) KEGG bioinformatics resource for plant genomics research. Methods Mol Biol **406:** 437–458

Métraux JP (2002) Recent breakthroughs in the study of salicylic acid biosynthesis. Trends Plant Sci **7:** 332–334

Mollá-Morales A, Sarmiento-Mañús R, Robles P, Quesada V, Pérez-Pérez JM, González-Bayón R, Hannah MA, Willmitzer L, Ponce MR, Micol JL (2011) Analysis of *ven3* and *ven6* reticulate mutants reveals the importance of arginine biosynthesis in Arabidopsis leaf development. Plant J **65:** 335–345

Niyogi KK, Fink GR (1992) Two anthranilate synthase genes in *Arabidopsis*: defense-related regulation of the tryptophan pathway. Plant Cell **4:** 721–733

Obata T, Matthes A, Koszior S, Lehmann M, Araújo WL, Bock R, Sweetlove LJ, Fernie AR (2011) Alteration of mitochondrial protein complexes in relation to metabolic regulation under short-term oxidative stress in Arabidopsis seedlings. Phytochemistry **72:** 1081–1091

Obayashi T, Hayashi S, Saeki M, Ohta H, Kinoshita K (2009) ATTED-II provides coexpressed gene networks for Arabidopsis. Nucleic Acids Res **37:** D987–D991

Overmyer K, Kollist H, Tuominen H, Betz C, Langebartels C, Wingsle G, Kangasjärvi S, Brader G, Mullineaux P, Kangasjärvi J (2008) Complex phenotypic profiles leading to ozone sensitivity in *Arabidopsis thaliana* mutants. Plant Cell Environ **31:** 1237–1249

Pavet V, Olmos E, Kiddle G, Mowla S, Kumar S, Antoniw J, Alvarez ME, Foyer CH (2005) Ascorbic acid deficiency activates cell death and disease resistance responses in Arabidopsis. Plant Physiol **139:** 1291–1303

Peltier JB, Emanuelsson O, Kalume DE, Ytterberg J, Friso G, Rudella A, Liberles DA, Söderberg L, Roepstorff P, von Heijne G, et al (2002) Central functions of the lumenal and peripheral thylakoid proteome of *Arabidopsis* determined by experimentation and genome-wide prediction. Plant Cell **14:** 211–236

Pérez-Pérez JM, Candela H, Micol JL (2009) Understanding synergy in genetic interactions. Trends Genet **25:** 368–376

Pérez-Pérez JM, Candela H, Robles P, López-Torrejón G, del Pozo JC, Micol JL (2010) A role for *AUXIN RESISTANT3* in the coordination of leaf growth. Plant Cell Physiol **51:** 1661–1673

Pérez-Pérez JM, Ponce MR, Micol JL (2002) The *UCU1 Arabidopsis* gene encodes a SHAGGY/GSK3-like kinase required for cell expansion along the proximodistal axis. Dev Biol **242:** 161–173

Ponce MR, Quesada V, Micol JL (1998) Rapid discrimination of sequences flanking and within T-DNA insertions in the *Arabidopsis* genome. Plant J **14:** 497–501

Potel F, Valadier MH, Ferrario-Méry S, Grandjean O, Morin H, Gaufichon L, Boutet-Mercey S, Lothier J, Rothstein SJ, Hirose N, et al (2009) Assimilation of excess ammonium into amino acids and nitrogen translocation in *Arabidopsis thaliana*—roles of glutamate synthases and carbamoylphosphate synthetase in leaves. FEBS J **276:** 4061–4076

Queval G, Issakidis-Bourguet E, Hoeberichts FA, Vandorpe M, Gakière B, Vanacker H, Miginiac-Maslow M, Van Breusegem F, Noctor G (2007) Conditional oxidative stress responses in the Arabidopsis photorespiratory mutant *cat2* demonstrate that redox state is a key modulator of daylength-dependent gene expression, and define photoperiod as a crucial factor in the regulation of H_2O_2-induced cell death. Plant J **52:** 640–657

Rédei GP, Hirono Y (1964) Linkage studies. Arabidopsis Information Service **1:** 9–10

Rosar C, Kanonenberg K, Nanda AM, Mielewczik M, Bräutigam A, Novák O, Strnad M, Walter A, Weber AP (2012) The leaf reticulate mutant *dov1* is impaired in the first step of purine metabolism. Mol Plant **5:** 1227–1241

Schmid M, Davison TS, Henz SR, Pape UJ, Demar M, Vingron M, Schölkopf B, Weigel D, Lohmann JU (2005) A gene expression map of Arabidopsis thaliana development. Nat Genet **37:** 501–506

Schubert M, Petersson UA, Haas BJ, Funk C, Schröder WP, Kieselbach T (2002) Proteome map of the chloroplast lumen of *Arabidopsis thaliana*. J Biol Chem **277:** 8354–8365

Schwacke R, Schneider A, van der Graaff E, Fischer K, Catoni E, Desimone M, Frommer WB, Flügge UI, Kunze R (2003) ARAMEMNON, a novel database for Arabidopsis integral membrane proteins. Plant Physiol **131:** 16–26

Serrano-Cartagena J, Candela H, Robles P, Ponce MR, Pérez-Pérez JM, Piqueras P, Micol JL (2000) Genetic analysis of *incurvata* mutants reveals three independent genetic operations at work in *Arabidopsis* leaf morphogenesis. Genetics **156:** 1363–1377

Sessions A, Burke E, Presting G, Aux G, McElver J, Patton D, Dietrich B, Ho P, Bacwaden J, Ko C, et al (2002) A high-throughput *Arabidopsis* reverse genetics system. Plant Cell **14:** 2985–2994

Stacklies W, Redestig H, Scholz M, Walther D, Selbig J (2007) pcaMethods—a bioconductor package providing PCA methods for incomplete data. Bioinformatics **23:** 1164–1167

Streatfield SJ, Weber A, Kinsman EA, Häusler RE, Li J, Post-Beittenmiller D, Kaiser WM, Pyke KA, Flügge UI, Chory J (1999) The phosphoenolpyruvate/phosphate translocator is required for phenolic metabolism, palisade cell development, and plastid-dependent nuclear gene expression. Plant Cell **11:** 1609–1622

Sun X, Feng P, Xu X, Guo H, Ma J, Chi W, Lin R, Lu C, Zhang L (2011) A chloroplast envelope-bound PHD transcription factor mediates chloroplast signals to the nucleus. Nat Commun **2:** 477

Szakonyi D, Moschopoulos A, Byrne ME (2010) Perspectives on leaf dorsoventral polarity. J Plant Res **123:** 281–290

Tamura K, Peterson D, Peterson N, Stecher G, Nei M, Kumar S (2011) MEGA5: molecular evolutionary genetics analysis using maximum likelihood, evolutionary distance, and maximum parsimony methods. Mol Biol Evol **28:** 2731–2739

Thimm O, Bläsing O, Gibon Y, Nagel A, Meyer S, Krüger P, Selbig J, Müller LA, Rhee SY, Stitt M (2004) MAPMAN: a user-driven tool to display genomics data sets onto diagrams of metabolic pathways and other biological processes. Plant J **37:** 914–939

Ulker B, Shahid Mukhtar M, Somssich IE (2007) The WRKY70 transcription factor of *Arabidopsis* influences both the plant senescence and defense signaling pathways. Planta **226:** 125–137

Van Ree K, Gehl B, Chehab EW, Tsai YC, Braam J (2011) Nitric oxide accumulation in Arabidopsis is independent of NOA1 in the presence of sucrose. Plant J **68:** 225–233

Vanacker H, Carver TL, Foyer CH (2000) Early H_2O_2 accumulation in mesophyll cells leads to induction of glutathione during the hypersensitive response in the barley-powdery mildew interaction. Plant Physiol **123:** 1289–1300

Vanderauwera S, Suzuki N, Miller G, van de Cotte B, Morsa S, Ravanat JL, Hegie A, Triantaphylidès C, Shulaev V, Van Montagu MC, et al (2011) Extranuclear protection of chromosomal DNA from oxidative stress. Proc Natl Acad Sci USA **108:** 1711–1716

Voll L, Häusler RE, Hecker R, Weber A, Weissenböck G, Fiene G, Waffenschmidt S, Flügge UI (2003) The phenotype of the *Arabidopsis cue1* mutant is not simply caused by a general restriction of the shikimate pathway. Plant J **36:** 301–317

Weckwerth W, Wenzel K, Fiehn O (2004) Process for the integrated extraction, identification and quantification of metabolites, proteins and RNA to reveal their co-regulation in biochemical networks. Proteomics **4:** 78–83

Wildermuth MC, Dewdney J, Wu G, Ausubel FM (2001) Isochorismate synthase is required to synthesize salicylic acid for plant defence. Nature **414:** 562–565

Willemsen V, Wolkenfelt H, de Vrieze G, Weisbeek P, Scheres B (1998) The *HOBBIT* gene is required for formation of the root meristem in the *Arabidopsis* embryo. Development **125:** 521–531

Winter D, Vinegar B, Nahal H, Ammar R, Wilson GV, Provart NJ (2007) An "Electronic Fluorescent Pictograph" browser for exploring and analyzing large-scale biological data sets. PLoS ONE **2:** e718

Yu F, Fu A, Aluru M, Park S, Xu Y, Liu H, Liu X, Foudree A, Nambogga M, Rodermel S (2007) Variegation mutants and mechanisms of chloroplast biogenesis. Plant Cell Environ **30:** 350–365

Zybailov B, Rutschow H, Friso G, Rudella A, Emanuelsson O, Sun Q, van Wijk KJ (2008) Sorting signals, N-terminal modifications and abundance of the chloroplast proteome. PLoS ONE **3:** e1994